NANO LETTERS

February 7, 2024
Volume 24, Number 5
pubs.acs.org/NanoLett

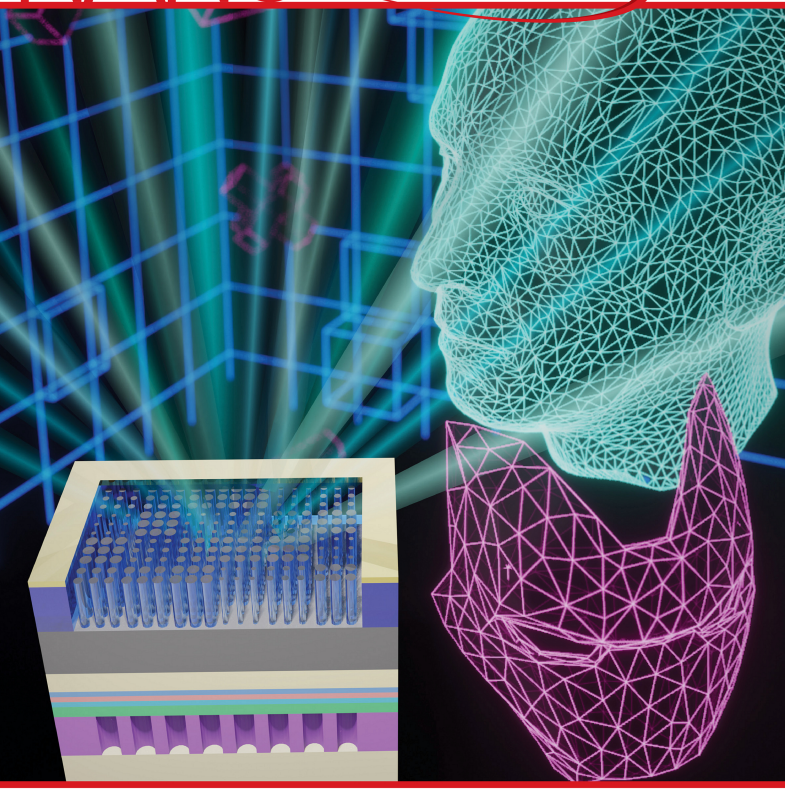

ACS Publications
Most Trusted. Most Cited. Most Read.

www.acs.org

NANO LETTERS

pubs.acs.org/NanoLett Letter

Metasurface- and PCSEL-Based Structured Light for Monocular Depth Perception and Facial Recognition

Wen-Cheng Hsu, Chia-Hsun Chang, Yu-Heng Hong,* Hao-Chung Kuo,* and Yao-Wei Huang*

Cite This: *Nano Lett.* 2024, 24, 1808−1815 Read Online

ACCESS | Metrics & More | Article Recommendations | Supporting Information

ABSTRACT: The novel depth-sensing system presented here revolutionizes structured light (SL) technology by employing metasurfaces and photonic crystal surface-emitting lasers (PCSELs) for efficient facial recognition in monocular depth-sensing. Unlike conventional dot projectors relying on diffractive optical elements (DOEs) and collimators, our system projects approximately 45,700 infrared dots from a compact 297-μm-dimention metasurface, drastically more spots (1.43 times) and smaller (233 times) than the DOE-based dot projector in an iPhone. With a measured field-of-view (FOV) of 158° and a 0.611° dot sampling angle, the system is lens-free and lightweight and boasts lower power consumption than vertical-cavity surface-emitting laser (VCSEL) arrays, resulting in a 5−10 times reduction in power. Utilizing a GaAs-based metasurface and a simplified optical architecture, this innovation not only addresses the drawbacks of traditional SL depth-sensing but also opens avenues for compact integration into wearable devices, offering remarkable advantages in size, power efficiency, and potential for widespread adoption.

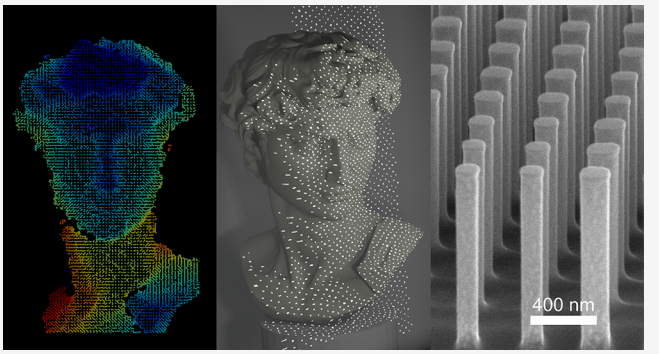

KEYWORDS: *metasurfaces, photonic crystal surface-emitting laser, structured light, depth sensing*

Downloaded via NATL YANG MING CHIAO TUNG UNIV on February 7, 2024 at 11:16:54 (UTC).
See https://pubs.acs.org/sharingguidelines for options on how to legitimately share published articles.

Three-dimensional (3D) surface imaging is recognized for its potential in computer vision, spatial computing, autonomous driving, and wearable devices. With high-speed computing advances, 3D imaging systems based on coherent light sources have emerged that extract depth information via various methods. Stereo vision, time-of-flight (ToF), and structured light (SL) categorize 3D imaging systems by depth estimation.[1−3] SL-based systems offer high resolution, large field-of-view (FOV), high frame rates, and low computational needs, suitable for smartphone integration for single-shot facial recognition.[4,5]

In an iPhone's dot projector, a pseudorandom beam pattern is emitted via a vertical-cavity surface-emitting laser (VCSEL) array, collimator, light-guide, and diffractive optical elements (DOEs).[6] Randomly arranged 366 spots were projected from a VCSEL-array chip. A multiorder diffraction pattern was then generated by passing through the DOE, resulting in over 32,000 dots in a FOV of 74°. The DOE's bulky size, narrow FOV, dot number, integration compatibility, and power consumption of the system pose challenges.

Metasurfaces, ultrathin optical elements modulating light,[7−10] replace bulky components, reducing optical system size and enabling novel features in depth sensors,[11] endoscopes,[12] tomography,[13] and virtual/augmented realities.[14] Metasurface designs for depth-sensing include light-field,[15] ToF,[16] and SL.[17−21] Yet, bulky lasers hinder chip integration and wearables. Integrating metasurfaces with a single VCSEL is achieved, but SL application efficacy is limited due to VCSEL features like larger divergence angles and output power.[22,23] Additionally, PCSELs provide an ultralow divergence angle in the meantime keeping a higher output power source,[24−26] providing the capability for integration with metasurfaces in a smaller form factor.[27,28]

In this paper, we present the demonstration of a metasurface-enhanced dot projector consisting of specifically a metasurface compatible with a PCSEL. As depicted in Figure 1(a), our meta-projector generates an SL-pattern composed of random dots captured by a camera. We perform disparity analysis to obtain 3D information and successfully achieve facial recognition in monocular depth-sensing. To overcome the limitations of commercial dot projectors, such as bulky size and complex optics, we have made significant design improvements. Instead of using a VCSEL array, bulky light guide, and collimation lenses, we employ a single PCSEL to generate a highly collimated light beam. Moreover, we replace

Received: December 19, 2023
Revised: December 28, 2023
Accepted: December 29, 2023
Published: January 10, 2024

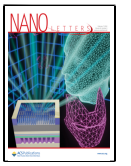

© 2024 American Chemical Society

https://doi.org/10.1021/acs.nanolett.3c05002
Nano Lett. 2024, 24, 1808−1815

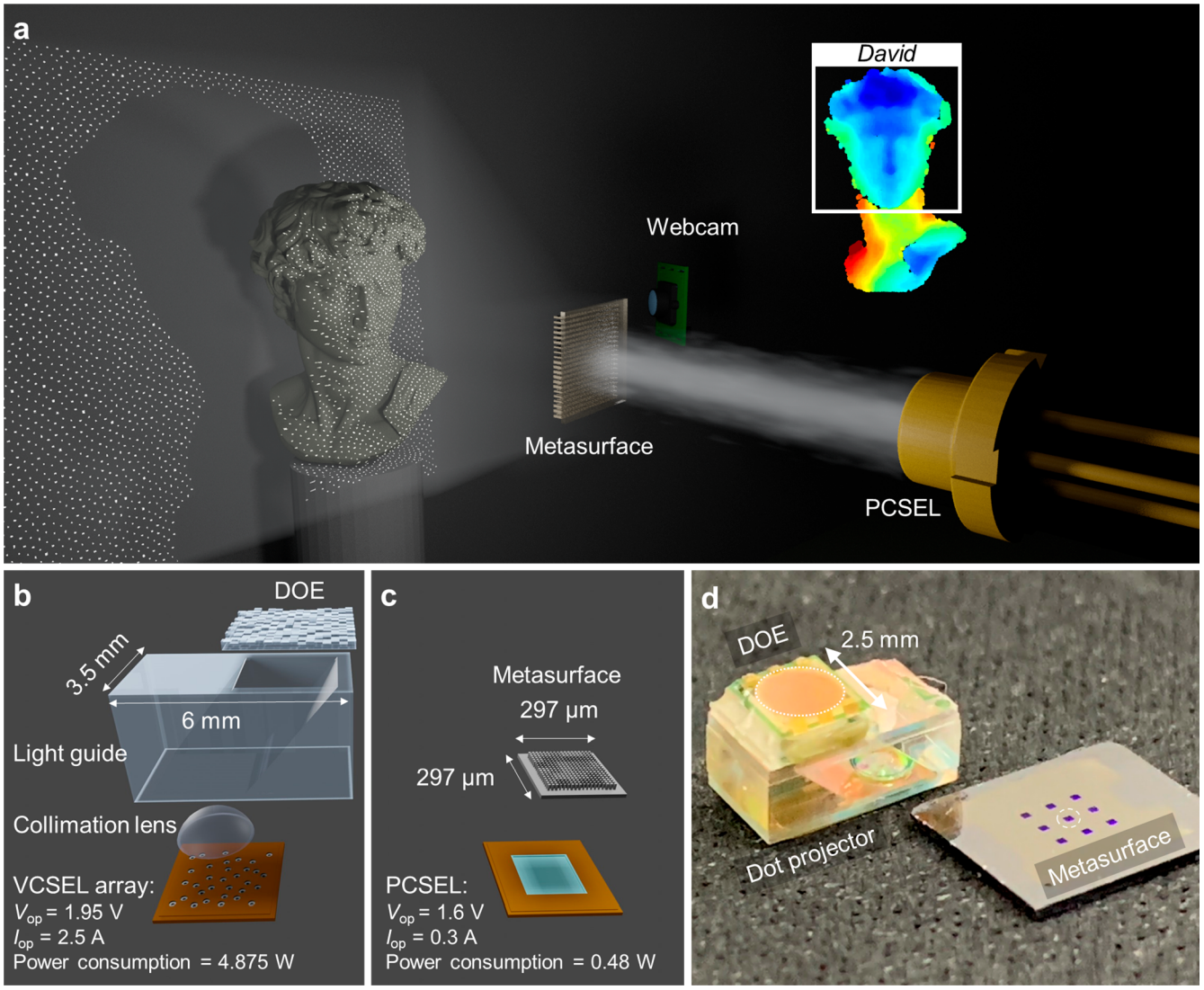

Figure 1. Illustration shows our proposed depth-sensing system and a comparison to the Face ID system in the Apple iPhone. (a) Schematic of single-shot SL system consisting of a camera and metasurface-enhanced dot projector. The system projects multi-infrared-dots from the PCSEL through metasurface hologram on the object for depth perception. (b) The dot projector module in iPhone composed with a chip of VCSEL-array, collimation lens, light guide, and DOE. (c) Our approach for the SL generation. (d) Size comparison of commercial dot projector and our metasurface samples.

the diffractive optical element (DOE) with a metasurface hologram, as illustrated in Figure 1(b),(c).

This design alteration results in lower power consumption and a more compact system. Figure 1(d) illustrates a significant difference in size between metasurface samples and a commercial dot projector found in an iPhone. The area of all optical components in the latter is 233 times larger than that of our metasurface sample. Additionally, the utilization of GaAs-based metasurfaces enhances the potential for integration with high-power laser sources like PCSEL.[24−26] This research demonstrates the capability of metasurfaces to enhance the efficiency and miniaturization of depth-sensing systems, particularly for wearable applications.

SL is generated by metasurface hologram and PCSEL, which is proposed from our previous work.[27,28] We design a polarization-insensitive metasurface with square nanopillars because the degree of linear polarization of our PCSEL is 0.534 (see Supporting Information Figure S1 for details). To generate clear dot images at a feasible distance between a cell phone and a person's face, the holographic dot images should be reconstructed at the far-field plane under the limitation of Fraunhofer diffraction. Additionally, it is necessary to have a larger number of dots in a holographic image to achieve higher angular resolution within a smaller area. Figure 2(a),(b) illustrate the trade-off between the imaging distance, metasurface dimension, and pixel and dot sampling angles. According to the Fraunhofer condition, the minimum distance (L) required to obtain clear dot images from the sample should be on the scale of a^2/λ, where a represents the dimension of the metasurface, and λ is the operation wavelength. The orange area shown in Figure 2(a) indicates the relationship between the required Fraunhofer condition and the dimensions of the metasurface. Furthermore, the accuracy of an object's surface, such as a person's face, using an SL-based depth-sensing system is influenced by the density of the dots illuminated on it. A higher dot density in a holographic image (or smaller sampling angle) leads to higher angular/spatial resolution in reconstructing 3D models.

https://doi.org/10.1021/acs.nanolett.3c05002
Nano Lett. 2024, 24, 1808−1815

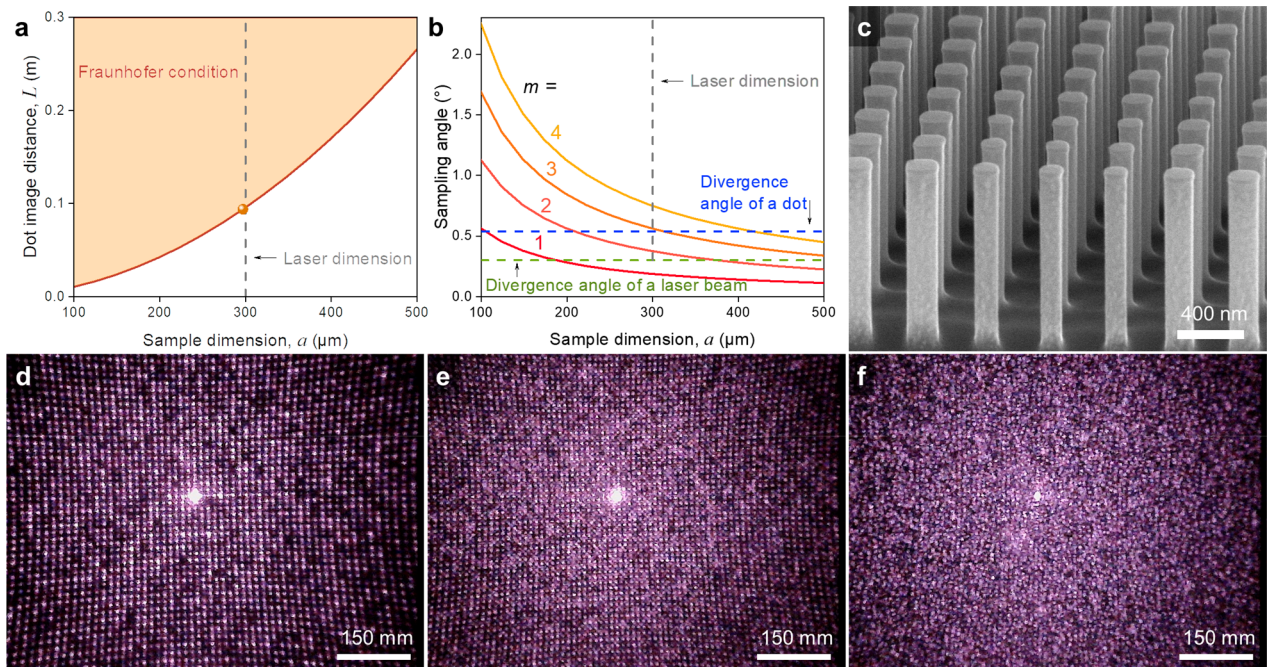

Figure 2. Structured light design principle and structured light of metasurface samples. (a) Fraunhofer diffraction distance corresponding to difference metasurface size. Orange ball: the minimum image distance of our metasurfaces is 9.4 cm. (b) The sample dimension versus sampling angle at a fixed pixel size. m represents the number of pixels between 2 neighbor feature dots. (c) Tiled (75°) SEM image of a metasurface sample. (d–f) Reconstructed SL-patterns corresponding to array arrangement (d and e) and random arrangement (f).

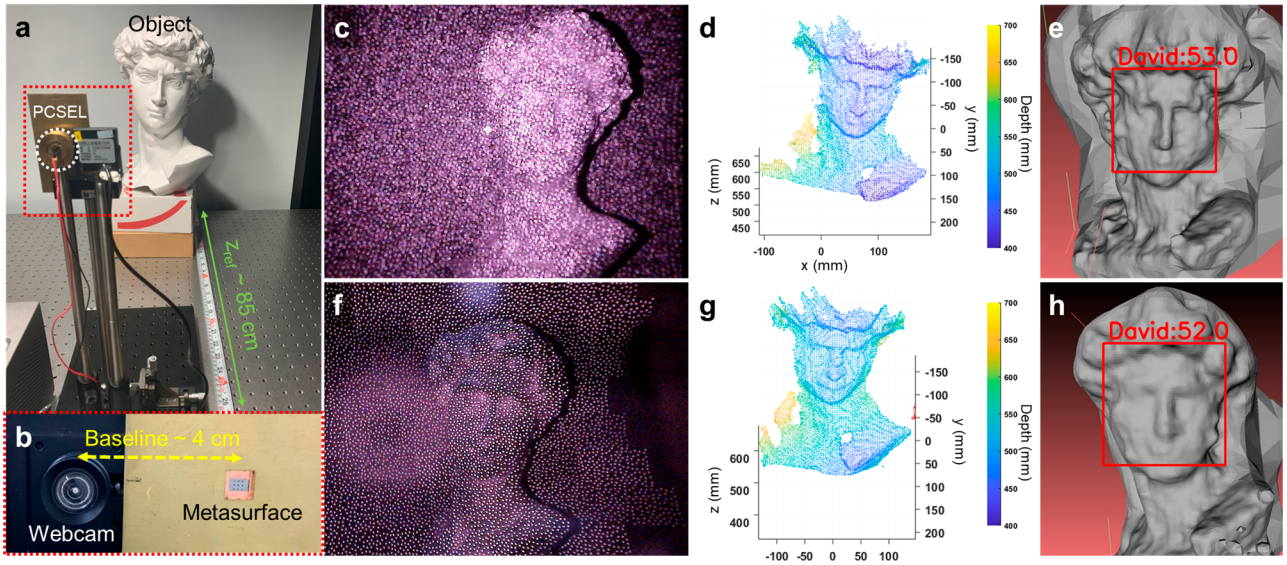

Figure 3. Setup and result of depth-sensing for facial recognition. (a) Setup of single-shot SL system. (b) Front view of the projector and webcam in (a). (c) Object image. (d) 3D reconstruction of *David*. (e) Facial recognition test generated by our system. (f–h) Depth-sensing and facial recognition results with the SL-pattern from an iPhone.

The average resolution of the dot image can be represented by the number of sampling pixels divided by the FOV_{0th} (usually has unit in pixels per degree), where the FOV_{0th} is $2 \times \sin^{-1}(\lambda/2\Lambda)$ denoting the horizontal angle range of a holographic image at the zeroth order diffraction, where Λ represents the dimension of a pixel. The pixel sampling angle (δ) represents the angle range that a pixel of a holographic image represents. Therefore, a higher resolution of the dot image indicates more precise feature points can be detected, and a smaller sampling angle is achieved. The FOV_{0th} of our holograms are designed at 56.7°. As the metasurface dimension increases, the pixel number increases, resulting in a smaller pixel sampling angle (red line in Figure 2(b)). Besides, the dot sampling angle (Δ), defined as the angle between 2 neighbor feature dots, determines the accuracy of the object's surface, which has relation with pixel sampling angle as $\Delta = m\delta$ and m is integer. Ideally, smaller dot sampling angle results in higher angular/spatial resolution. However, a wider divergence angle of laser would enhance the feature size of dots, which leads to lower recognizable in each dot. The relation in sample dimension, dot sampling angle (Δ), and pixel sampling angle (δ, where $m = 1$) are visualized as Figure 2(b) (see Supporting

https://doi.org/10.1021/acs.nanolett.3c05002
Nano Lett. 2024, 24, 1808−1815

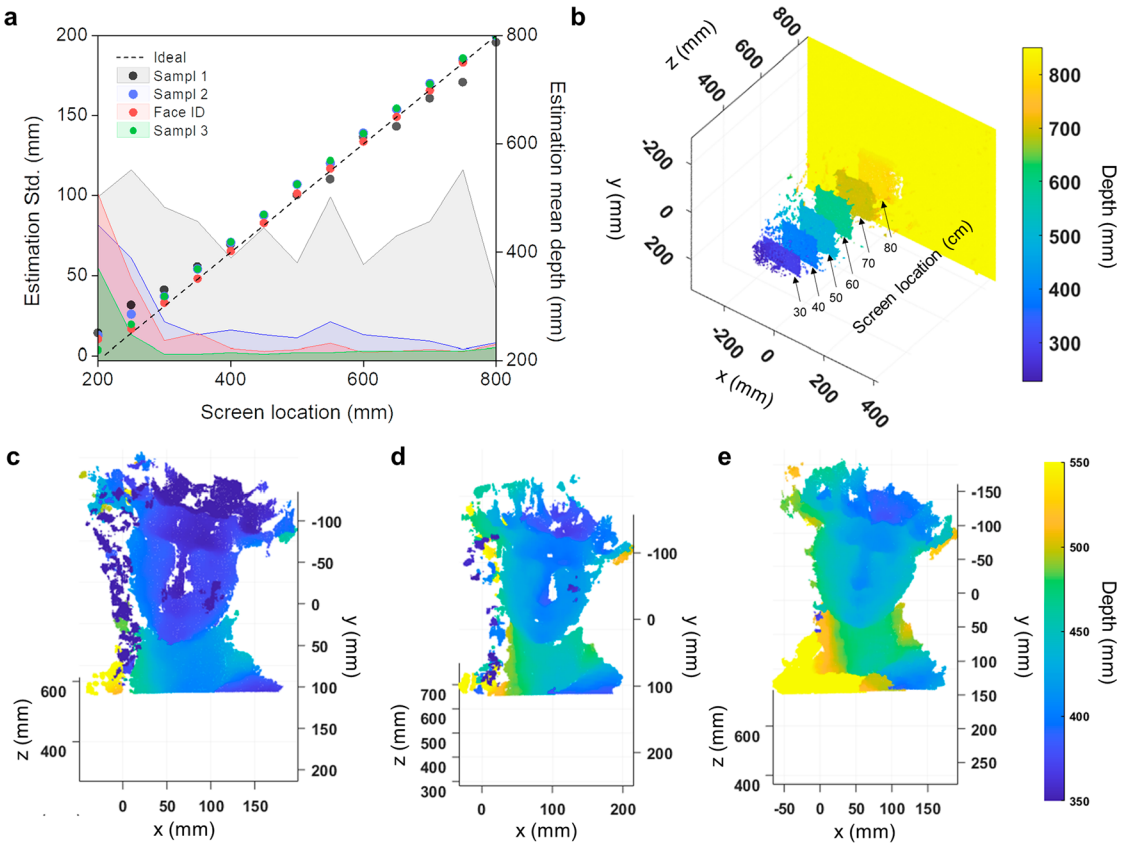

Figure 4. Reliability and accuracy of working distance in our structured light system. (a) The standard viewing screen location versus the estimated screen depth and the corresponding standard deviation. (b) The reconstructed 3D model of texture less screen from 30−80 cm. (c) The reconstruction point cloud of *David* for sample 1. (d) The reconstruction point cloud of *David* by sample 2. (e) The reconstruction point cloud of *David* by sample 3.

Information Figure S2 for details). In an ideal scenario, higher resolution (smaller sampling angle) would require a larger metasurface area, but this also leads to a greater Fraunhofer diffraction distance. These conditions are not ideal for miniaturizing the device and can limit the working distance in face recognition applications. To satisfy the face recognition range of 20−60 cm and the emitting window size of PCSEL (schematics shown in Supporting Information Figure S3), area of our metasurfaces is determined as 297^2 μm^2.

In our demonstration, we presented three samples with different types of SL-pattern generations to compare their depth-sensing abilities. Sample 1 consists of 25,700 dots (m = 4) arranged in a square lattice. Sample 2 has denser dots (45,700 dots, m = 3) arranged in a square lattice, and sample 3 has a similar density as sample 2 but in a random arrangement (43,500 dots, $3 \leq m \leq 4$) (see Supporting Information Figure S4 and Table S1 for details). Figure 2(c) displays a scanning electron microscopy (SEM) image of a metasurface sample, revealing vertical side walls, a height of 858 nm, and square-shaped pillars (see Supporting Information Figure S5 for a detailed fabrication process). Figure 2(d)−(f) shows the reconstructed images projected onto a projection curtain located 85 cm away from the samples (as reference image), demonstrating the differences in density and arrangement of the dots. We also performed experiments to analyze the SL-pattern's variation at different projection distances by studying the propagation path of dots. The results confirm that the imaging-distance relationship adheres to the Fraunhofer condition (Supporting Information Figures S6). Furthermore, the measured FOV reaches 158° (see Supporting Information Figures S7 for detailed experimental results).

Another significant advantage of using a PCSEL in our experiment, as opposed to a VCSEL-array in commercial dot projectors, is ultrasmall divergence angle (0.300°) and lower power consumption and. These features of PCSEL lead our proposed system no requirement of collimator lens and a power consumption of 0.48 W (I_{op} = 0.3A, V_{op} = 1.6 V), which is 5−10 times lower than VCSEL-array used in commercial dot projector (see Supporting Information Table S2 for detailed laser operation conditions).

We utilized a single-shot SL system to validate the performance of our meta-projector. The methodology employed to obtain depth information in a single-shot SL system is referred to previous work.[28−31] Figure 3(a),(b) displays a real setup of our depth-sensing system, where the distance of projection curtain (z_{ref}) is 85 cm, baseline is 4 cm, and the distance between meta-hologram and PCSEL is ∼1 cm (beam profile of PCSEL at this distance is shown in Supporting Information Figure S3f). The depth perception process of an object includes (1) generation of disparity image from reference image and object image by employing the block matching algorithm; (2) generation of depth image by analyzing the disparity image and applying the approximation of the triangular relationship; and (3) generation of 3D coordinates of the point cloud from depth image where pixel coordinate is transformed to global coordinate. The detailed depth perception process is in the "Methods" section. Figure 3(c),(d) corresponds to captured object image (with sample

https://doi.org/10.1021/acs.nanolett.3c05002
Nano Lett. 2024, 24, 1808−1815

Table 1. Comparison of Our Approach and State-of-the-Art with Impact Parameters and Figure of Merit

	face ID	ref 18	ref 19	ref 20	ref 23	our sample 2
diffraction order			±4	±47	±1	±1
dot number, N (#)	32 K	441	69	10 K	9	45.7 K
field of view, FOV (deg)	74	30	120	180	20	158
area, A (μm^2)	$\pi \times 1250^2$	2500^2	250^2	500^2	$\pi \times 100^2$	297^2
material		a-Si	a-Si	a-Si	GaAs	GaAs
operation wavelength, λ (nm)	940	940	850/940	633	980	940
sampling angle, Δ (deg)	0.642		15	1.757	10	0.611
FoM(# / μm^2)	0.751		8.83×10^{-3}	4.10	5.73×10^{-4}	134

3) and 3D point cloud of model generated by compacted emitter with metasurface and PCSEL (see Supporting Information Figure S8 and Movie S1 for corresponding experimental results).

In addition to the quantitative analysis of the 3D point clouds of *David*, we performed surface reconstruction and facial recognition to further evaluate the results where the process is shown in the "Methods" section. The facial recognition test results are shown in Figure 3(e).

After that, we employed the same experimental methodology but with SL-pattern generated by using the dot projection of Face ID system in an iPhone X (hereinafter referred to as Face ID), and the object image is shown in Figure 3(f). The corresponding 3D reconstruction and facial recognition tests are shown in Figure 3(g),(h). It is clear the object in 3D point cloud is *David* in both ways (Figure 3(d),(g)). The facial recognition results (Figure 3(e),(h)) are also classified to correct class with similar confidence score, which are 53 and 52 respectively. We also employed the same face recognition methodology to recognize the images of reconstruction of *David* from refs 32 and 33 and a photograph of our *David* model. These images are classified as *David* and scored 52, 54, and 44. The confidence scores assigned after labeling represent the level of confidence in the facial recognition system with values ranging from 0 to 100. A score below 50 suggests higher reliability, while a score above 85 indicates a larger margin of error. This analysis demonstrates that both the SL-based depth reconstruction approach using sample 3 and the dot projection of Face ID system yield accurate results in identifying and categorizing the facial features of *David*.

To evaluate the performance of the metasurface samples in our SL depth-sensing systems, we conducted an experiment to measure the relationship between a standard textureless viewing screen location (as a ground-truth depth) and the estimated distance obtained from our SL system. We compared results by using SL patterns from samples 1−3 and from Face ID. This experiment aimed to quantify the properties of different samples and investigate the ideal conditions for achieving accurate diffraction imaging and feature matching.

The experiment detected the screen position from 20−80 cm (see Supporting Information Figure S9 for detailed experimental results). Figure 4(a) presents the results and analysis, where the colored dots represent the estimated mean depth at different screen positions. The mean depth was calculated by averaging the depth values corresponding to the area of the screen in the depth map. It can be observed from Figure 4(a) that the estimated mean depths from samples 1−3 and Face ID exhibit a linear relationship and align closely with the ideal condition (black dashed line) from 30−80 cm.

In Figure 4(a), each colored shadow area represents the corresponding standard deviation of the estimated mean depth. It was observed that the results from sample 2 exhibited a smaller deviation compared to sample 1. This can be attributed to the denser arrangement of dots in the SL-pattern, which provides more sampling points for depth estimation in the algorithm. Samples 2 and 3 and Face ID have similar dot densities, but they differ in arrangement. Consequently, sample 3 demonstrated an even smaller deviation compared to sample 2 and Face ID. The difference in lower deviation and the more precise performance can be attributed to random arrangement of dots because of easier calculation of disparity image through block matching.[34]

The visualization of the reconstructed 3D point cloud of the screen at different distances measured by using sample 3 is depicted in Figure 4(b) and demonstrates a lower deviation at 30−80 cm. This highlights the accuracy of depth-sensing in sample 3 reaches the level of dot projection of Face ID. Figure 4(c)−(e) shows the reconstruction point clouds of *David* located at 40 cm corresponding to samples 1, 2, and 3. These results meet the conclusion in Figure 4(a) as well, indicating depth-sensing with sample 3 has less error. Overall, the smaller standard deviation observed in sample 3 indicates its superior performance in terms of depth-sensing accuracy, making it the most precise among the tested samples (see Supporting Information Figures S10 and S11 for further examples).

We list the specification of Face ID, related works, and our approach in Table 1. We also introduce a Figure of Merit (FoM) to quantitatively assess the performance of SL techniques, focusing on a greater number of emitting dots (N), a larger FOV, a smaller size area (A), and a smaller dot sampling angle (Δ). The FoM is calculated using the formula:

$$FoM = \frac{N \times FOV}{A \times \Delta}$$

In our work, we have achieved a FoM value of 134, which is more higher than other grating based SL,[18−20,23] and SL technique implemented in the Face ID system. The higher FoM in our evaluation indicates ultrasmall size but maintains the precise reconstruction shape.

We have considered various parameters, including divergence angle of a dot, which may impact the dot projector's performance. However, we have successfully demonstrated the depth-sensing capabilities of our system and passed the facial recognition test under the specified design conditions. It is because we can employ a threshold value on demand to digitally identify a dot sampling angle in the algorithm. Notably, the zero order of the SL-pattern plays an unimportant role in our depth-sensing system (Supporting Information Figure S12) because it has similar dot size compared to other.

https://doi.org/10.1021/acs.nanolett.3c05002
Nano Lett. 2024, 24, 1808−1815

This study presents a novel depth-sensing system that combines a metasurface and a PCSEL as a dot projector. Through an experimental evaluation, we have demonstrated the effectiveness and quality of our proposed system. The results show an accurate distance estimation and high-quality point cloud generation for various objects. The effectiveness of the system is evaluated using the *FoM*, which considers parameters such as the number of emitting dots, field of view, size area, and sampling angle. Our proposed system achieves a higher *FoM* value, indicating superior performance in terms of a smaller size area while maintaining accurate depth-sensing capability.

Compared with existing depth-sensing systems, our proposed system offers several advantages. First, it is a compact and cost-effective system that can be integrated into a single chip using the flip-chip process of PCSEL. Employing PCSEL as the light source eradicates the necessity for extra lenses, thereby streamlining both complexity and size. This effectively tackles the persistent challenge arising from constraints related to the space between the metasurface and the VCSEL array, as well as the issue of insufficient phase fineness encountered in the seamless integration of the metasurface on single VCSEL.[23] Second, the metasurface enables the generation of customizable and versatile light patterns, expanding the system's applicability. Additionally, the system achieves lower power consumption compared with VCSEL-array-based dot projectors, enhancing energy efficiency. The system has a certain limitations. First, the divergence angle of dots increases after passing through a metasurface. Consequently, the PCSEL's divergence angle must be sufficiently small; otherwise, the dot sampling angle increases, resulting in a diminished capacity for object exploration and a weakened ability to outline object contours. Second, the beam shape of the PCSEL should be circular (e.g., Gaussian beam or circle flat-top beam); otherwise, it may lead to distortion and deformation of the diffraction patterns.

In conclusion, we introduce a theoretical balance among the laser emitting area, divergence angle, dot image distance, and appropriate sampling angle for facial depth perception. Our depth-sensing system utilizing metasurface and PCSEL presents a simple, cost-effective, and versatile solution. The system's compact size, low power consumption, and customizable light patterns make it a promising technology for future depth-sensing applications. Its potential applications span various fields including facial recognition, robotics, and extended reality.

METHODS

Depth Perception. We employed the block matching algorithm for generation of the disparity image, which used the reference image and object image to do feature matching. The reference image is the captured image by projected the SL pattern on a projection curtain and object image is captured image by projected the SL pattern on *David* or a standard flat white viewing screen (EDU-VS1, Thorlabs). The depth image is then estimated by analyzing the disparity image and applying the approximation of the triangular relationship (see Supporting Information Figure S8 for a detailed mechanism). After extracting the depth information, the next step involves transforming the 3D coordinates of the point cloud from pixel coordinate to global coordinate. This transformation process utilizes the intrinsic matrix, which is obtained from Zhang's calibration method (see the "Camera Calibration" section). All the depth calculations are implemented with Matlab (R2021a version) on a computer (CPU: AMD Ryzen Threadripper 3960X 24-Core Processor, GPU: NVIDIA GeForce RTX 2060). The average calculation time is obtained by calculation of 7 individual cases. These steps from reading images to a reconstructed model take an average time of 0.608 s. It takes an average time of 0.809 s to display a 3D point cloud.

Surface Reconstruction and Facial Recognition. To begin, we utilized MeshLab to convert the point cloud data into a mesh surface, enabling us to perform surface reconstruction. Subsequently, we trained a facial recognition classifier using distinct categories of faces in OpenCV. The data set includes photos of *David*, Albert Einstein, Elon Musk, Jen-Hsun "Jensen" Huang, Steve Jobs, and Wen-Cheng Hsu (one of the authors).

Camera Calibration. Camera calibration is a crucial step in our SL system to achieve accurate and reliable 3D models in the global coordinate system. We employ Zhang's calibration method, which is a widely used approach for estimating the intrinsic and extrinsic parameters of a camera. To perform camera calibration, we placed a calibration target with known geometry at various positions and orientations within the scene. We capture multiple images of the calibration target from different viewpoints using the camera. The intrinsic parameters, such as the focal length, principal point, and lens distortion coefficients, as well as the extrinsic parameters, which describe the camera's position and orientation in the scene, are then estimated. The estimation of these parameters is achieved by minimizing the error in retraction between the detected corner points in the calibration images and the ideal corner points of the calibration target. This optimization process ensures that the camera model accurately represents the real-world geometry. The details of derivation and calibration are shown in Supporting Information Figure S13.

ASSOCIATED CONTENT

Data Availability Statement

The data are available under restricted access for non-commercial use, and access can be obtained from the corresponding authors upon reasonable request. The codes that support the findings of this study are available upon reasonable request from the corresponding authors.

Supporting Information

The Supporting Information is available free of charge at https://pubs.acs.org/doi/10.1021/acs.nanolett.3c05002.

Additional details of meta-atoms, meta-holograms, sampling angle, PCSEL, VCSEL array, SL-patterns, fabrication process, Fraunhofer condition, measured SL-patterns, measured FOV, depth estimation mechanism, depth sensing of different models, and zero order effect (PDF)

Movie S1: 3D point cloud of *David* (MP4)

AUTHOR INFORMATION

Corresponding Authors

Yu-Heng Hong − *Semiconductor Research Center, Hon Hai Research Institute, Taipei 11492, Taiwan;* orcid.org/0000-0001-9935-5861; Email: enoch.yh.hong@foxconn.com

Hao-Chung Kuo − *Department of Photonics, College of Electrical and Computer Engineering, National Yang Ming Chiao Tung University, Hsinchu 30010, Taiwan;*

https://doi.org/10.1021/acs.nanolett.3c05002
Nano Lett. 2024, 24, 1808−1815

Semiconductor Research Center, Hon Hai Research Institute, Taipei 11492, Taiwan; Email: hckuo0206@nycu.edu.tw

Yao-Wei Huang − *Department of Photonics, College of Electrical and Computer Engineering, National Yang Ming Chiao Tung University, Hsinchu 30010, Taiwan*; orcid.org/0000-0001-8983-413X; Email: ywh@nycu.edu.tw

Authors

Wen-Cheng Hsu − *Department of Photonics, College of Electrical and Computer Engineering, National Yang Ming Chiao Tung University, Hsinchu 30010, Taiwan; Semiconductor Research Center, Hon Hai Research Institute, Taipei 11492, Taiwan*

Chia-Hsun Chang − *Department of Photonics, College of Electrical and Computer Engineering, National Yang Ming Chiao Tung University, Hsinchu 30010, Taiwan*

Complete contact information is available at: https://pubs.acs.org/10.1021/acs.nanolett.3c05002

Author Contributions

Y.-W.H. and W.-C.H. initiated the study. W.-C.H. performed the numerical calculation and simulation. C.-H.C. fabricated metasurface samples. W.-C.H. and Y.-H.H. performed the optical experiments. H.-C.K., Y.-W.H., W.-C.H., and Y.-H.H. contributed required materials and analysis tools. W.-C.H. and Y.-W.H. analyzed experimental data and wrote the manuscript. H.-C.K., Y.-H.H., Y.-W.H, W.-C.H., and C.-H.C. discussed the results and commented on the manuscript.

Funding

National Science and Technology Council in Taiwan (Grant Nos. 110−2622−8-A49−008-SB, 111−2622−8-A49−021-SB, and 110−2112-M-A49−034-MY3).

Notes

The authors declare no competing financial interest.

■ ACKNOWLEDGMENTS

This work is supported by the National Science and Technology Council in Taiwan (Grant Nos. 110-2622-8-A49-008-SB, 111-2622-8-A49-021-SB, and 110-2112-M-A49-034-MY3). We also acknowledge support from the Ministry of Education in Taiwan under the Yushan Young Scholar Program. We acknowledge the Semiconductor Research Center, Hon Hai Research Institute, for their technical support. This work was performed in part at the Nano Facility Center and Center for Nano Science and Technology in NYCU. We also acknowledge Prof. Din Ping Tsai, Prof. Tien-Chang Lu, Prof. Peichen Yu, and the Taiwan Semiconductor Research Institute (TSRI) for their technical discussion.

■ REFERENCES

(1) Yang, S.-P.; Seo, Y.-H.; Kim, J.-B.; Kim, H.; Jeong, K.-H. Optical MEMS Devices for Compact 3D Surface Imaging Cameras. *Micro Nano Syst. Lett.* **2019**, *7* (1), 8.

(2) Song, Z.; Tang, S.; Gu, F.; Shi, C.; Feng, J. DOE-Based Structured-Light Method for Accurate 3D Sensing. *Opt. Lasers Eng.* **2019**, *120*, 21−30.

(3) Gu, F.; Cao, H.; Song, Z.; Xie, P.; Zhao, J.; Liu, J. Dot-Coded Structured Light for Accurate and Robust 3D Reconstruction. *Appl. Opt.* **2020**, *59* (33), 10574.

(4) Pribanić, T.; Petković, T.; Đonlić, M.; Angladon, V.; Gasparini, S. 3D Structured Light Scanner on the Smartphone. In Image Analysis and Recognition. *Lect. Notes Comput. Sci.* **2016**, *9730*, 443−450.

(5) Zhang, S. High-Speed 3D Shape Measurement with Structured Light Methods: A Review. *Opt. Lasers Eng.* **2018**, *106*, 119−131.

(6) Mor, Z. Integrated Structured-Light Projector Comprising Light-Emitting Elements on a Substrate. US9825425B2, November 21, 2017. https://patents.google.com/patent/US9825425B2/ko (accessed 2023−08−10).

(7) Yu, N.; Capasso, F. Flat Optics with Designer Metasurfaces. *Nat. Mater.* **2014**, *13* (2), 139−150.

(8) Hsiao, H.-H.; Chu, C. H.; Tsai, D. P. Fundamentals and Applications of Metasurfaces. *Small Methods* **2017**, *1* (4), 1600064.

(9) Engelberg, J.; Levy, U. The Advantages of Metalenses over Diffractive Lenses. *Nat. Commun.* **2020**, *11* (1), 1991.

(10) Jiang, Q.; Jin, G.; Cao, L. When Metasurface Meets Hologram: Principle and Advances. *Adv. Opt. Photonics* **2019**, *11* (3), 518−576.

(11) Guo, Q.; Shi, Z.; Huang, Y.-W.; Alexander, E.; Qiu, C.-W.; Capasso, F.; Zickler, T. Compact Single-Shot Metalens Depth Sensors Inspired by Eyes of Jumping Spiders. *Proc. Natl. Acad. Sci. U. S. A.* **2019**, *116* (46), 22959−22965.

(12) Pahlevaninezhad, H.; Khorasaninejad, M.; Huang, Y.-W.; Shi, Z.; Hariri, L. P.; Adams, D. C.; Ding, V.; Zhu, A.; Qiu, C.-W.; Capasso, F.; Suter, M. J. Nano-Optic Endoscope for High-Resolution Optical Coherence Tomography in Vivo. *Nat. Photonics* **2018**, *12* (9), 540−547.

(13) Pahlevaninezhad, M.; Huang, Y.-W.; Pahlevani, M.; Bouma, B.; Suter, M. J.; Capasso, F.; Pahlevaninezhad, H. Metasurface-Based Bijective Illumination Collection Imaging Provides High-Resolution Tomography in Three Dimensions. *Nat. Photonics* **2022**, *16* (3), 203−211.

(14) Li, Z.; Lin, P.; Huang, Y.-W.; Park, J.-S.; Chen, W. T.; Shi, Z.; Qiu, C.-W.; Cheng, J.-X.; Capasso, F. Meta-Optics Achieves RGB-Achromatic Focusing for Virtual Reality. *Sci. Adv.* **2021**, *7* (5), No. eabe4458.

(15) Chen, M. K.; Liu, X.; Wu, Y.; Zhang, J.; Yuan, J.; Zhang, Z.; Tsai, D. P. A Meta-Device for Intelligent Depth Perception. *Adv. Mater.* **2023**, *35*, 2107465.

(16) Juliano Martins, R.; Marinov, E.; Youssef, M. A. B.; Kyrou, C.; Joubert, M.; Colmagro, C.; Gâté, V.; Turbil, C.; Coulon, P.-M.; Turover, D.; Khadir, S.; Giudici, M.; Klitis, C.; Sorel, M.; Genevet, P. Metasurface-Enhanced Light Detection and Ranging Technology. *Nat. Commun.* **2022**, *13* (1), 5724.

(17) Li, Z.; Dai, Q.; Mehmood, M. Q.; Hu, G.; Yanchuk, B. L.; Tao, J.; Hao, C.; Kim, I.; Jeong, H.; Zheng, G.; Yu, S.; Alù, A.; Rho, J.; Qiu, C.-W. Full-Space Cloud of Random Points with a Scrambling Metasurface. *Light Sci. Appl.* **2018**, *7* (1), 63.

(18) Li, N.; Fu, Y. H.; Dong, Y.; Hu, T.; Xu, Z.; Zhong, Q.; Li, D.; Lai, K. H.; Zhu, S.; Lin, Q.; Gu, Y.; Singh, N. Large-Area Pixelated Metasurface Beam Deflector on a 12-Inch Glass Wafer for Random Point Generation. *Nanophotonics* **2019**, *8* (10), 1855−1861.

(19) Ni, Y.; Chen, S.; Wang, Y.; Tan, Q.; Xiao, S.; Yang, Y. Metasurface for Structured Light Projection over 120° Field of View. *Nano Lett.* **2020**, *20* (9), 6719−6724.

(20) Kim, G.; Kim, Y.; Yun, J.; Moon, S.-W.; Kim, S.; Kim, J.; Park, J.; Badloe, T.; Kim, I.; Rho, J. Metasurface-Driven Full-Space Structured Light for Three-Dimensional Imaging. *Nat. Commun.* **2022**, *13* (1), 5920.

(21) Jing, X.; Zhao, R.; Li, X.; Jiang, Q.; Li, C.; Geng, G.; Li, J.; Wang, Y.; Huang, L. Single-Shot 3D Imaging with Point Cloud Projection Based on Metadevice. *Nat. Commun.* **2022**, *13* (1), 7842.

(22) Xie, Y.-Y.; Ni, P.-N.; Wang, Q.-H.; Kan, Q.; Briere, G.; Chen, P.-P.; Zhao, Z.-Z.; Delga, A.; Ren, H.-R.; Chen, H.-D.; Xu, C.; Genevet, P. Metasurface-Integrated Vertical Cavity Surface-Emitting Lasers for Programmable Directional Lasing Emissions. *Nat. Nanotechnol.* **2020**, *15* (2), 125−130.

(23) Wang, Q.; Ni, P.; Xie, Y.; Kan, Q.; Chen, P.; Fu, P.; Deng, J.; Jin, T.; Chen, H.; Lee, H. W. H.; Xu, C.; Genevet, P. On-Chip Generation of Structured Light Based on Metasurface Optoelectronic Integration. *Laser Photonics Rev.* **2021**, *15* (3), 2000385.

(24) Imada, M.; Chutinan, A.; Noda, S.; Mochizuki, M. Multidirectionally Distributed Feedback Photonic Crystal Lasers. *Phys. Rev. B* **2002**, *65* (19), 195306.
(25) Hirose, K.; Liang, Y.; Kurosaka, Y.; Watanabe, A.; Sugiyama, T.; Noda, S. Watt-Class High-Power, High-Beam-Quality Photonic-Crystal Lasers. *Nat. Photonics* **2014**, *8* (5), 406−411.
(26) Yoshida, M.; De Zoysa, M.; Ishizaki, K.; Tanaka, Y.; Kawasaki, M.; Hatsuda, R.; Song, B.; Gelleta, J.; Noda, S. Double-Lattice Photonic-Crystal Resonators Enabling High-Brightness Semiconductor Lasers with Symmetric Narrow-Divergence Beams. *Nat. Mater.* **2019**, *18* (2), 121−128.
(27) Chen, L.-R.; Chang, C.-J.; Hong, K.-B.; Weng, W.-C.; Chuang, B.-H.; Huang, Y.-W.; Lu, T.-C. Static Beam Steering by Applying Metasurfaces on Photonic-Crystal Surface-Emitting Lasers. *J. Light. Technol.* **2022**, *40* (21), 7136−7141.
(28) Hsu, W.-C.; Chang, C.-H.; Hong, Y.-H.; Kuo, H.-C.; Huang, Y.-W. Compact Structured Light Generation Based on Meta-Hologram PCSEL Integration. *Discovery Nano* **2023**, *18* (1), 87.
(29) Wang, G.; Yin, X.; Pei, X.; Shi, C. Depth Estimation for Speckle Projection System Using Progressive Reliable Points Growing Matching. *Appl. Opt.* **2013**, *52* (3), 516.
(30) Donlic, M.; Petkovic, T.; Pribanic, T. On Tablet 3D Structured Light Reconstruction and Registration. *IEEE Int. Conf. Comput. Vision Workshops* **2017**, 2462−2471.
(31) Zhang, Z. A. Flexible New Technique for Camera Calibration. *IEEE Trans. Pattern Anal. Mach. Intell.* **2000**, *22* (11), 1330−1334.
(32) Yin, W.; Hu, Y.; Feng, S.; Huang, L.; Kemao, Q.; Chen, Q.; Zuo, C. Single-Shot 3D Shape Measurement Using an End-to-End Stereo Matching Network for Speckle Projection Profilometry. *Opt. Express* **2021**, *29* (9), 13388.
(33) Bao, W.; Xiao, X.; Xu, Y.; Zhang, X. Reference Image Based Phase Unwrapping Framework for a Structured Light System. *Opt. Express* **2018**, *26* (22), 29588.
(34) Zuo, C.; Zhang, X.; Hu, Y.; Yin, W.; Shen, D.; Zhong, J.; Zheng, J.; Chen, Q. Has 3D Finally Come of Age? – An Introduction to 3D Structured-Light Sensor. *Infrared Laser Eng.* **2020**, *49* (3), 303001−303001.

https://doi.org/10.1021/acs.nanolett.3c05002
Nano Lett. 2024, 24, 1808−1815